



## Article

# Magnetic Dipole and Thermophoretic Particle Deposition Impact on Bioconvective Oldroyd-B Fluid Flow over a Stretching Surface with Cattaneo–Christov Heat Flux

Seemab Bashir <sup>1</sup>, Muhammad Ramzan <sup>2,\*</sup> , Hassan Ali S. Ghazwani <sup>3</sup>, Kottakaran Sooppy Nisar <sup>4</sup> , C. Ahamed Saleel <sup>5</sup> and Anas Abdelrahman <sup>6</sup>

<sup>1</sup> Department of Mathematics, Air University, Islamabad 44000, Pakistan; sabbasi354736@yahoo.com

<sup>2</sup> Department of Computer Science, Bahria University, Islamabad 44000, Pakistan

<sup>3</sup> Department of Mechanical Engineering, Faculty of Engineering, Jazan University, Jazan 45124, Saudi Arabia; hghazwani@jazanu.edu.sa

<sup>4</sup> Department of Mathematics, College of Arts and Sciences, Prince Sattam bin Abdulaziz University, Wadi Aldawaser 11991, Saudi Arabia; drnisarks1@gmail.com

<sup>5</sup> Department of Mechanical Engineering, College of Engineering, King Khalid University, Asir-Abha 61421, Saudi Arabia; ahamedsaleel@gmail.com

<sup>6</sup> Mechanical Engineering, Faculty of Engineering & Technology, Future University in Egypt, New Cairo 11835, Egypt; anas.mohamed@fue.edu.eg

\* Correspondence: mramzan@bahria.edu.pk



**Citation:** Bashir, S.; Ramzan, M.; Ghazwani, H.A.S.; Nisar, K.S.; Saleel, C.A.; Abdelrahman, A. Magnetic Dipole and Thermophoretic Particle Deposition Impact on Bioconvective Oldroyd-B Fluid Flow over a Stretching Surface with Cattaneo–Christov Heat Flux. *Nanomaterials* **2022**, *12*, 2181. <https://doi.org/10.3390/nano12132181>

Academic Editor: Mikhail Sheremet

Received: 31 May 2022

Accepted: 23 June 2022

Published: 25 June 2022

**Publisher's Note:** MDPI stays neutral with regard to jurisdictional claims in published maps and institutional affiliations.



**Copyright:** © 2022 by the authors. Licensee MDPI, Basel, Switzerland. This article is an open access article distributed under the terms and conditions of the Creative Commons Attribution (CC BY) license (<https://creativecommons.org/licenses/by/4.0/>).

**Abstract:** This study emphasizes the performance of two-dimensional electrically non-conducting Oldroyd-B fluid flowing across a stretching sheet with thermophoretic particle deposition. The heat and mass transfer mechanisms are elaborated in the presence of a magnetic dipole, which acts as an external magnetic field. The fluid possesses magnetic characteristics due to the presence of ferrite particles. The gyrotactic microorganisms are considered to keep the suspended ferromagnetic particles stable. Cattaneo–Christov heat flux is cogitated instead of the conventional Fourier law. Further, to strengthen the heat transfer and mass transfer processes, thermal stratification and chemical reaction are employed. Appropriate similarity transformations are applied to convert highly nonlinear coupled partial differential equations into non-linear ordinary differential equations (ODEs). To numerically solve these ODEs, an excellent MATLAB bvp4c approach is used. The physical behavior of important parameters and their graphical representations are thoroughly examined. The tables are presented to address the thermophoretic particle velocity deposition, rate of heat flux, and motile microorganisms' density number. The results show that the rate of heat transfer decreases as the value of the thermal relaxation time parameter surges. Furthermore, when the thermophoretic coefficient increases, the velocity of thermophoretic deposition decreases.

**Keywords:** magnetic dipole; gyrotactic microorganism; thermophoretic particle deposition; bioconvection; Cattaneo–Christov heat flux

## 1. Introduction

In many industrial processes, working liquids have diverse rheological characteristics, whose viscoelasticity and viscosity can continually be changed and molded by exerting forces and external variables, such as stress, strain, timeframe, and temperature. These non-Newtonian fluid models are further distinguished by a nonlinear relationship between stress and deformation rates. The rate, the integral, and the differential types are the three primary classifications for these fluids. Because of the ease of mathematical modeling, many scholars have been interested in the problems of differential type fluids. In differential type models, shear stress is stated as velocity components. Nonetheless, there have been fewer attempts in the case of rate-type fluids. The Maxwell fluid model, one of the most well-known rate type fluid models, has a limited scope with

only relaxation time information. However, the Oldroyd-B fluid model [1] has both relaxation and retardation time features. Ibrahim et al. [2] studied the mixed convection flow of Oldroyd-B nanofluid flow with the Cattaneo–Christov heat and mass flux model by adding mixed convection and third-order slip. Hayat et al. [3] used an exponentially stretching sheet to analyze the boundary layer flow effects of Oldroyd-B fluid. Ramzan et al. [4] discovered the effects of the magnetic dipole on ferromagnetic Oldroyd-B nanofluid flow. An Oldroyd-B nanofluid flow with heat generation and stratification are elaborated by Waqas et al. [5]. The multiple characteristics of this essential non-Newtonian fluid have attracted many researchers' interests [6–13].

Thermophoretic particle deposition (TPD) in a liquid flow is significant in a variety of engineering procedures, such as powdered coal burner, heat exchanger, nuclear reactor protection, building ventilation systems, and air cleaners. Numerous classifications of particles act differently when subjected to a temperature gradient, resulting in the thermophoresis phenomenon. In thermophoresis, small minute particles suspended in a non-isothermal gas will attain a velocity, and this process significantly upsurges the deposition velocity of minute particles in the direction of declining temperature, but the large particles are unaffected by this process. Thermophoresis permits tiny particles to settle on a cold chilly surface. The velocity of the gas molecules in the cold region is usually less than that coming from the warm area of the particles. The particles with high velocity collide with the other particles. Then the velocity is attained by the particles due to this momentum difference, and this velocity is usually defined as the thermophoretic velocity. The thermophoretic force is exerted by a temperature gradient on suspended particles. Alam et al. [14] investigated two-dimensional steady MHD flow with thermophoresis and variable suction over a semi-infinite inclined plate in the addition of thermal radiation. Damseh et al. [15] studied thermophoresis particle deposition with the addition of MHD on a vertical surface with mixed convection. Gowda et al. [16] investigated thermophoresis particle deposition on a vertically upward downward-moving disk with a hybrid nanofluid. Kumar [17] explored the impact of the magnetic dipole on thermophoretic particle deposition, selecting Maxwell fluid over a stretching sheet. Additionally, the influence of thermophoretic particle deposition under various conditions is noticed by many authors [18–23].

Magnetohydrodynamics (MHDs) studies the dynamics of electrically conducting fluids in particular. Ferrofluids are a family of magnetizable liquids that have unique properties and a significant impact on technology. Ferrofluids are suspended magnetic particles generally measuring 10 nm distributed in a carrier liquid. Avionics, robotics, lasers, aerodynamics, computer peripherals, nuclear plants, and drawing plastic are some of the notable industrial uses of these fluids. The wide-ranging benefits of these fluids have prompted scientists and academics to mobilize their research on this specific subject. Neuringer [24] examined the magnetic dipole effects on stagnation flow point in ferrofluid at first. The presence of magnetic dipole in a ferrofluid flow was studied by Andersson and Valnes [25]. Waqas et al. [26] investigated the ferrofluid and magnetic dipole on a Carreau fluid using the Buongiorno model. In addition, references [27–35] address new work on ferromagnetic fluid with a magnetic dipole.

A significant element of heat transport that has been researched by many scientists is stratification. Temperature changes, concentration fluctuations, or liquids of various densities cause it in flow fields. Many engineering applications make use of the principle of stratification due to higher energy performance and efficiencies, such as industrial composition, atmospheric density stratification, and solar energy. Hayat et al. [36] investigated the effects of thermal and solutal stratification on the two-dimensional flow of an MHD Jeffrey nanofluid with the addition of mixed convection. Sandeep et al. [37] investigated dual stratification and MHD effects on a stretching sheet with the addition of a non-uniform heat source/sink. Ramzan et al. [38] studied double stratification on Williamson MHD nanofluid flow in three dimensions with Cattaneo–Christov heat flux. Rehman et al. [39] explored the mixed convection, stratification, and heat generation/absorption effects on

Eyring–Powell nanofluid flow over an inclined stretching cylinder. Stratification with different flow regimes is studied by many other researchers [17,36,38,40–47].

The above-mentioned literature survey indicates that plenty of research is available considering various characteristics of nanofluid flow. However, insufficient analyses are taken into account while concentrating on electrically non-conducting Oldroyd-B nanofluid with magnetic dipole effects over a stretched sheet in addition to thermal stratification; this discussion channel becomes more focused if we add the Cattaneo–Christov heat flux model and thermophoretic particle deposition in the fluid. In this exploration, all the above-quoted aspects are added to the envisioned model. In addition, gyrotactic microorganisms of Oldroyd-B nanofluid are also employed in order to stabilize the suspended ferromagnetic particles. Furthermore, the heat transfer mechanism is better explained in the presence of a first-order chemical reaction in the current study. Using suitable similarity transformations, the governing system of a strongly nonlinear system is numerically determined. The impacts of various physical parameters on velocity, temperature, concentration, and motile gyrotactic microorganisms are calculated via graphing. The principal objective of the presented model is to answer the subsequent questions:

- What are the effects of relaxation retardation time on the velocity profile?
- How are temperature profiles affected by thermal stratification parameters?
- How is the concentration profile influenced by introducing thermophoretic particle deposition?
- How does magnetic dipole influence the skin friction coefficient?
- What is the effect of the highest swimming speed of microorganisms on the density number of motile microorganisms?

Table 1 shows the contrast comparison of the present work and the already available published work, which shows the uniqueness of the present work.

**Table 1.** A comparison of present work with closely comparable published research efforts.

Authors	Oldroyd-B	Magnetic Dipole	Thermophoretic Particle Deposition	Cattaneo–Christov Heat Flux	Thermal Stratification	Gyrotactic Microorganisms	Chemical Reaction
[10]	Yes	No	No	Yes	Yes	No	Yes
[17]	No	Yes	Yes	No	No	No	Yes
[29]	No	Yes	Yes	Yes	Yes	No	No
Present	Yes	Yes	Yes	Yes	Yes	Yes	Yes

## 2. Mathematical Formulation

Over a stretched sheet, a two-dimensional Oldroyd-B incompressible fluid is integrated. Due to the force applied to the sheet at  $y = 0$ , the sheet is stretched along the  $x$ -axis at the velocity  $u_w = cx$ . A magnetic dipole is placed in the framework on the vertical axis at a distance  $a$  from the sheet. Furthermore, the magnetic dipole produces a magnetic field in the positive direction to saturate the working ferrofluid. The stretched sheet temperature  $T_w$  is lower as compared to Curie temperature  $T_c$ , and at this temperature, the magnetic effect vanishes. The variable temperature is  $T_w(x) = T_0 + n_1x$ , whereas  $T_0$  is the reference temperature. Figure 1 portrays the geometrical inflow structure.

The model equations are expressed with the above-cited assumptions [10–12,29]:

$$\frac{\partial \tilde{u}}{\partial x} + \frac{\partial \tilde{v}}{\partial y} = 0, \quad (1)$$

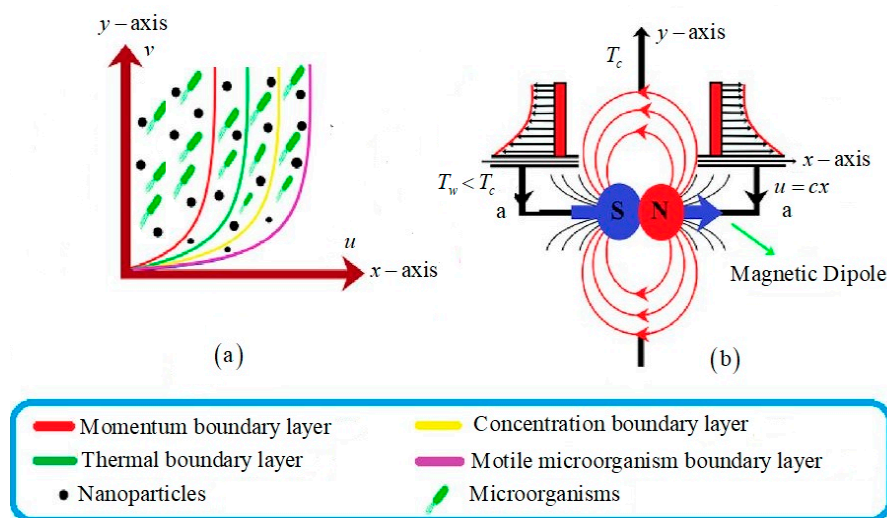


Figure 1. The geometry of the flow (a) boundary layers configuration (b) magnetic dipole placement.

$$\tilde{u} \frac{\partial \tilde{u}}{\partial x} + \tilde{v} \frac{\partial \tilde{u}}{\partial y} + \tilde{\Lambda}_1 \left( \tilde{u}^2 \frac{\partial^2 \tilde{u}}{\partial x^2} + \tilde{v}^2 \frac{\partial^2 \tilde{u}}{\partial y^2} + 2\tilde{u}\tilde{v} \frac{\partial^2 \tilde{u}}{\partial x \partial y} \right) = \frac{\mu}{\rho} \frac{\partial^2 \tilde{u}}{\partial y^2} - \frac{\mu_0 M}{\rho} \left( \frac{\partial \tilde{H}}{\partial x} \right) + v \tilde{\Lambda}_2 \left( \tilde{u} \frac{\partial^3 \tilde{u}}{\partial x \partial y} - \frac{\partial \tilde{u}}{\partial x} \frac{\partial^2 \tilde{u}}{\partial y^2} + \tilde{v} \frac{\partial^3 \tilde{u}}{\partial y^3} - \frac{\partial \tilde{u}}{\partial y} \frac{\partial^2 \tilde{v}}{\partial y^2} \right), \tag{2}$$

$$\tilde{u} \frac{\partial T}{\partial x} + \tilde{v} \frac{\partial T}{\partial y} = \alpha^* \left( \frac{\partial^2 T}{\partial x^2} + \frac{\partial^2 T}{\partial y^2} \right) - \lambda_H \left( \tilde{u} \frac{\partial \tilde{u}}{\partial x} \frac{\partial T}{\partial x} + \tilde{v} \frac{\partial \tilde{v}}{\partial y} \frac{\partial T}{\partial y} + \tilde{u} \frac{\partial \tilde{v}}{\partial x} \frac{\partial T}{\partial y} + \tilde{v} \frac{\partial \tilde{u}}{\partial y} \frac{\partial T}{\partial x} + 2\tilde{u}\tilde{v} \frac{\partial^2 T}{\partial x \partial y} + \tilde{u}^2 \frac{\partial^2 T}{\partial x^2} + \tilde{v}^2 \frac{\partial^2 T}{\partial y^2} \right) - \frac{(T\mu_0)\partial M}{(\rho C_p)\partial T} \left( \tilde{u} \frac{\partial \tilde{H}}{\partial x} + \tilde{v} \frac{\partial \tilde{H}}{\partial y} \right), \tag{3}$$

$$\tilde{u} \frac{\partial C}{\partial x} + \tilde{v} \frac{\partial C}{\partial y} = D \left( \frac{\partial^2 C}{\partial x^2} + \frac{\partial^2 C}{\partial y^2} \right) - \frac{\partial}{\partial y} (V_T C) - k_1^* (C - C_c), \tag{4}$$

$$\tilde{u} \frac{\partial n}{\partial x} + \tilde{v} \frac{\partial n}{\partial y} + \frac{bW_e}{C_w - C_o} \left( \frac{\partial}{\partial y} \left[ n \frac{\partial C}{\partial y} \right] \right) = D_m \frac{\partial^2 n}{\partial y^2}, \tag{5}$$

with applicable boundary conditions

$$\tilde{u}|_{y=0} = cx, T|_{y=0} = T_o + n_1 x = T_w, \tilde{v}|_{y=0} = 0, C|_{y=0} = C_w, n|_{y=0} = n_w, \tilde{u}|_{y \rightarrow \infty} = 0, T|_{y \rightarrow \infty} \rightarrow T_c = T_o + n_2 x, C|_{y \rightarrow \infty} \rightarrow C_o, n|_{y \rightarrow \infty} \rightarrow n_o, \tag{6}$$

where  $k_1^*$  is the chemical reaction rate,  $\tilde{\Lambda}_1$  and  $\tilde{\Lambda}_2$  are relaxation and retardation times of the material, respectively,  $\alpha^*$  is the thermal diffusivity,  $\lambda_H$  is thermal relaxation time coefficient,  $V_T$  is thermophoretic velocity,  $W_e$  is highest swimming speed of microorganisms,  $D_m$  is the microorganisms' diffusion coefficient, and  $n$  shows the concentration of microorganisms.

### 3. Magnetic Dipole

The magnetic scalar potential for Oldroyd-B liquid flow is given by:

$$\varphi = \frac{\gamma_0}{2\pi} \frac{x}{(y + e)^2 + x^2}. \tag{7}$$

Components of the magnetic field are

$$\tilde{H}_x = - \frac{(y + e)^2 - x^2}{\left( (y + e)^2 + x^2 \right)^2} \frac{\gamma_0}{2\pi} = - \frac{\partial \varphi}{\partial x}, \tag{8}$$

$$\tilde{H}_y = \frac{2x(y+e)}{(x^2+(y+e)^2)^2} \frac{\gamma_0}{2\pi} = -\frac{\partial\varphi}{\partial y}. \tag{9}$$

Taking

$$\tilde{H} = -\nabla\varphi, \quad \tilde{H} = \sqrt{\left(\frac{\partial\varphi}{\partial y}\right)^2 + \left(\frac{\partial\varphi}{\partial x}\right)^2}, \tag{10}$$

gives

$$\frac{\partial\tilde{H}}{\partial y} = \left(\frac{\gamma_0}{2\pi}\right) [-2(y+e)^{-3} + 4x^2(y+e)^{-5}], \tag{11}$$

$$\frac{\partial\tilde{H}}{\partial x} = -\left(\frac{\gamma_0}{2\pi}\right) [2x(y+e)^{-4}]. \tag{12}$$

A linear relation between  $M$  and  $T$  is as follows:

$$M = K(T_c - T). \tag{13}$$

#### 4. Thermophoretic Particle Deposition

The thermophoretic particle velocity  $V_T$  is given as:

$$V_T = -\nu\kappa^*T_y\frac{1}{T}. \tag{14}$$

Here,  $\kappa^*$  has the ranges of  $0.2 \leq \kappa^* \leq 1.2$ .  $\nu\kappa^*$  and  $\kappa^*$  are recognized as:

$$\kappa^* = \frac{2C_s\left(\frac{\lambda_g}{\lambda_p} + C_tK_n\right)\left[1 + K_n\left(C_1 + C_2e^{-\frac{C_3}{K_n}}\right)\right]}{(1 + 3C_mK_n)\left(1 + 2C_tK_n + \frac{\lambda_g}{\lambda_p}\right)}. \tag{15}$$

$\lambda_p, \lambda_g$  are base liquid and diffused particle thermal conductivities, respectively. Additionally,  $C_m = 1.146, C_1 = 1.2, C_s = 1.147, C_2 = 0.41, C_3 = 0.88,$  and  $C_t = 2.20$ .

#### 5. Similarity Transformation

Introducing dimensionless coordinates:

$$(\xi, \eta) = \left(\sqrt{\frac{c}{\nu}}x, \sqrt{\frac{c}{\nu}}y\right), \quad \tilde{u} = cxf'(\eta), \quad \tilde{v} = -\sqrt{c\nu}f(\eta), \tag{16}$$

$$\theta(\xi, \eta) = \frac{T_c - T}{T_0 - T_w} = \theta_1(\eta) + \xi^2\theta_2(\eta) = T_c - (T_0 - T_w)\left[\theta_1(\eta) + \xi^2\theta_2(\eta)\right], \tag{17}$$

$$\Omega(\xi, \eta) = \frac{C_c - C}{C_0 - C_w} = \Omega_1(\eta) + \xi^2\Omega_2(\eta) = C_c - (C_0 - C_w)\left[\Omega_1(\eta) + \xi^2\Omega_2(\eta)\right], \tag{18}$$

$$\chi(\xi, \eta) = \frac{n_c - n}{n_0 - n_w} = \chi_1(\eta) + \xi^2\chi_2(\eta) = n_c - (n_0 - n_w)\left[\chi_1(\eta) + \xi^2\chi_2(\eta)\right], \tag{19}$$

Using the above, Equation (1) is fulfilled, and Equations (2)–(6) take the form

$$f''' - f'^2 - \frac{2\beta\theta_1}{(\eta + \alpha)^4} + ff'' + B_2(f''^2 - ff^{iv}) + B_1(2ff'f''' - f^2f''') = 0, \tag{20}$$

$$\theta_1'' + 4\theta_2 - \text{Pr}\left(f'\theta_1 - f\theta_1' + S_t f' + \lambda_h\left(\begin{matrix} f^2\theta_1'' + f'^2S_t - ff''\theta_1 \\ + f'^2\theta_1 - ff''S_t - ff'\theta_1' \end{matrix}\right)\right) - \frac{2\lambda\beta f(\theta_1 + \varepsilon)}{(\eta + \alpha)^3} = 0, \tag{21}$$

$$\theta_2'' - \text{Pr}\left(3f'\theta_2 - f\theta_2' - \lambda_h\left(\begin{matrix} f^2\theta_2'' + 5f'^2\theta_2 \\ - 3ff'\theta_2' - 3ff''\theta_2 \end{matrix}\right)\right) + \frac{2\lambda\beta f\theta_2}{(\eta + \alpha)^3} + \lambda\beta(\theta_1 + \varepsilon)\left[-\frac{4f}{(\eta + \alpha)^5} + \frac{2f'}{(\eta + \alpha)^4}\right] = 0, \tag{22}$$

$$\Omega_1'' + Sc(f\Omega_1' - \gamma\Omega_1) + 2\Omega_2 + Sc\kappa^*N_t \frac{(N_c - \Omega_1)}{(1 - N_t\theta_1)} \left[ \theta_1'' - \frac{\Omega_1'\theta_1'}{(N_c - \Omega_1)} + \frac{2N_t(\theta_1)^2}{(1 - N_t\theta_1)} \right] = 0, \tag{23}$$

$$\begin{aligned} \Omega_2'' + Sc(f\Omega_2' - 2f'\Omega_2 - \gamma\Omega_2) - Sc\kappa^*N_t \frac{(N_c - \Omega_2)}{(1 - N_t\theta_2)} \\ \left[ \theta_2'' + \frac{\Omega_1'\theta_2' + \Omega_2'\theta_1' - \Omega_2\theta_1''}{(N_c - \Omega_2)} - \left( N_t \frac{\Omega_2(\theta_1)^2 + 2\theta_1'\theta_2'}{(1 - N_t\theta_2)} \right) \right] = 0, \end{aligned} \tag{24}$$

$$\chi_1'' + Le f\chi_1' - Pe(\chi_1'\Omega_1' - (\delta - \chi_1)\Omega_1'') = 0, \tag{25}$$

$$\chi_2'' - Le(f\chi_2' - 2f'\chi_2) - Pe(-\chi_2'\Omega_1' - \chi_1'\Omega_2' - (\delta - \chi_1)\Omega_2'' + \chi_2\Omega_1'') = 0, \tag{26}$$

with

$$\begin{aligned} f(0) = 0, \quad f'(0) = 1, \quad \theta_1(0) = 1 - S_t, \\ \theta_2(0) = 0, \quad \Omega_1(0) = 1, \quad \Omega_2(0) = 0, \quad \chi_1(0) = 0, \quad \chi_2(0) = 0, \\ f'(\infty) = 0, \quad \theta_1(\infty) = 0, \quad \theta_2(\infty) = 0, \quad \Omega_1(\infty) = 0, \quad \Omega_2(\infty) = 0, \\ \chi_1(\infty) = 0, \chi_2(\infty) = 0, \end{aligned} \tag{27}$$

and distinct dimensionless parameters are translated as under:

$$\begin{aligned} \beta = \mu_o K \frac{\gamma_o(T_o - T_w)\rho}{2\pi\mu^2}, \quad B_1 = \tilde{\Lambda}_1 c, \quad B_2 = \tilde{\Lambda}_2 c, \quad \alpha = \sqrt{\frac{c}{v}} e, \quad \lambda = \frac{c\mu^2}{k\rho(T_o - T_w)}, \quad S_t = \frac{n_2}{n_1}, \\ Sc = \frac{v}{D}, \quad \lambda_h = c\lambda_H \varepsilon = \frac{T_c}{T_o - T_w}, \quad \lambda_m = c\lambda_M, \quad N_c = \frac{C_c}{C_o - C_w}, \quad N_t = \frac{T_o - T_w}{T_c}, \quad \gamma = \frac{k_1}{c}, \\ Pr = \frac{\mu C_p}{k}, \quad Pe = \frac{bW_e}{D_m}, \quad Le = \frac{v}{D_m}, \quad \delta = \frac{n_c}{n_o - n_w}. \end{aligned} \tag{28}$$

### 6. Quantities of Practical Interest

The dimensional form of Nusselt number  $N_u$ , thermophoretic particle deposition velocity  $V_d^*$ , and local Stanton number  $St_r$ , and the number density of microorganisms  $N_n$  are given by:

$$N_u = - \frac{xq_h}{k(T_o - T_w)} \Big|_{y=0} \quad \text{with} \quad q_h = -k \frac{\partial T}{\partial y} \Big|_{y=0}, \tag{29}$$

$$V_d^* = \frac{V_d}{v}. \quad \text{where} \quad V_d = \frac{xq_m}{(C_o - C_w)} \Big|_{y=0} \quad \text{and} \quad q_m = -D \frac{\partial C}{\partial y} \Big|_{y=0}, \tag{30}$$

$$V_d^* = -Re^{\frac{1}{2}} St_r, \quad \text{where} \quad St_r = - \frac{xq_m}{v(C_o - C_w)} \Big|_{y=0} \quad \text{and} \quad q_m = -D \frac{\partial C}{\partial y} \Big|_{y=0}, \tag{31}$$

$$N_n = - \frac{xq_n}{D_m(n_o - n_w)} \Big|_{y=0} \quad \text{where} \quad q_n = -D_m \frac{\partial n}{\partial y} \Big|_{y=0}, \tag{32}$$

Dimensionless  $N_u$ ,  $V_d^*$ ,  $St_r$ , and  $N_n$  are as follows:

$$\begin{aligned} \frac{N_u}{\sqrt{Re}} = -(\theta_1'(0) + \zeta^2\theta_2'(0)), \quad V_d^* = - \frac{(\Omega_1'(0) + \zeta^2\Omega_2'(0))}{Sc}, \quad \sqrt{Re} St_r = - \frac{(\Omega_1'(0) + \zeta^2\Omega_2'(0))}{Sc}, \\ \frac{N_n}{\sqrt{Re}} = -(\chi_1'(0) + \zeta^2\chi_2'(0)), \end{aligned} \tag{33}$$

where  $Re = \frac{cx^2}{v}$  is the local Reynolds number.

### 7. Numerical Solution

For the obtained Equations (20)–(27), the MATLAB bvp4c scheme is implemented. New variables are assumed for this purpose as:

$$\begin{aligned}
 f(\eta) &= y_1, f'(\eta) = y_2, f''(\eta) = y_3, f^{iv}(\eta) = y_4, f^v(\eta) = y_5, \theta_1(\eta) = y_6, \theta_1''(\eta) = y_7, \theta_2(\eta) = y_8, \theta_2'(\eta) = y_9, \theta_2''(\eta) = y_{10}, \Omega_1(\eta) = y_{11}, \Omega_1'(\eta) = y_{12}, \Omega_1''(\eta) = y_{13}, \chi_1(\eta) = y_{14}, \chi_1'(\eta) = y_{15}, \chi_1''(\eta) = y_{16}, \\
 \Omega_2(\eta) &= y_{11}, \Omega_2'(\eta) = y_{12}, \Omega_2''(\eta) = y_{13}, \chi_2(\eta) = y_{14}, \chi_2'(\eta) = y_{15}, \chi_2''(\eta) = y_{16}, \\
 \chi_2(\eta) &= y_{15}, \chi_2'(\eta) = y_{16}, \chi_2''(\eta) = y_{17}.
 \end{aligned}
 \tag{34}$$

The use of the above expressions gives the following transformation to the equations:

$$yy_1 = \frac{1}{y_1} \left[ y_3^2 + \frac{1}{B_2} \left( y_4 - \frac{2\beta}{(\eta + \alpha)^4} y_5 - y_2^2 + y_1 y_3 + B_1 (2y_1 y_2 y_4 - y_1^2 y_4) \right) \right], \tag{35}$$

$$yy_2 = \frac{1}{(1 - \lambda_h Pr y_1^2)} \left[ Pr \left( y_2 y_5 + S_t y_2 - y_1 y_6 + \lambda_h \left( \begin{array}{c} y_1^2 y_5 + S_t y_2^2 \\ -y_1 y_2 y_6 - y_1 y_3 y_5 \\ -S_t y_1 y_3 \end{array} \right) \right) - 4y_7 + \frac{2\lambda\beta y_1 (y_5 + \varepsilon)}{(\eta + \alpha)^3} \right], \tag{36}$$

$$yy_3 = \frac{1}{(1 + \lambda_n Pr y_1^2)} \left[ Pr (3y_2 y_7 - y_1 y_8 + \lambda_h (5y_2^2 y_7 - 3y_1 y_2 y_8 - 3y_1 y_3 y_7)) - \frac{2\lambda\beta}{(\eta + \alpha)^3} y_7 - \lambda\beta (y_5 + \varepsilon) \left( \frac{2y_2}{(\eta + \alpha)^4} - \frac{4y_1}{(\eta + \alpha)^5} \right) \right], \tag{37}$$

$$yy_4 = Sc(\gamma y_9 - y_1 y_{10}) - 2y_{11} - Sc\kappa^* N_t \frac{(N_c - y_9)}{(1 - N_t y_5)} \left[ yy_2 - \frac{y_6 y_{10}}{(N_c - y_9)} + \frac{2N_t y_5^2}{(1 - N_t y_5)} \right], \tag{38}$$

$$yy_5 = Sc(2y_2 y_{11} - \gamma y_{11} - y_1 y_{12}) + \frac{Sc\kappa^* N_t}{(1 - N_t y_7)} \left[ \begin{array}{c} y_6 y_{12} - y_{10} y_8 - y_2 y_{11} - y_3 (N_c - y_9) \\ + \frac{N_t (-2y_6 y_8 (N_c - y_9) - y_6^2 y_{11})}{(1 - N_t y_7)} \end{array} \right], \tag{39}$$

$$yy_6 = -Le y_1 y_{14} + Pe (y_{14} y_{10} - (\delta - y_{13}) yy_4), \tag{40}$$

$$yy_7 = 2Le y_2 y_{15} - Le y_1 y_{16} + Pe (-y_{10} y_{16} - y_{14} y_{12} - (\delta - y_{13}) yy_5 + y_{15} yy_4). \tag{41}$$

With the transformed BCs:

$$\begin{aligned}
 y_1(0) &= 0, y_2(0) = 1, y_2(\infty) = 0, y_5(0) = 1 - S_t, y_5(\infty) = 0, y_7(0) = 0, \\
 y_7(\infty) &= 0, y_9(0) = 0, y_9(\infty) = 0, y_{11}(0) = 0, y_{11}(\infty) = 0, y_{13}(0) = 0, \\
 y_{13}(\infty) &= 0, y_{15}(0) = 0, y_{15}(\infty) = 0.
 \end{aligned}
 \tag{42}$$

### 8. Results and Discussion

This section depicts a graphical sketch of the involved parameters.

#### 8.1. Velocity Profile

Figure 2 shows how the material parameter  $B_1$  affects the velocity profile. On large estimations of the relaxation time constant  $B_1$ , velocity is reduced, as seen in Figure 2. The rise in the  $B_1$  is the reason for the reduction in velocity and causes a slower recuperation rate. The reason behind this is that for large estimates of  $B_1$ , a slower recovery process is observed, causing the thickness layer to expand at a slower pace. The effects of  $B_2$  on  $f'(\eta)$  are seen in Figure 3. When  $B_2$  is raised, the fluid flow is improved.

#### 8.2. Temperature Profile

The features of thermally stratified parameter  $S_t$  against  $\theta_1(\eta)$  are presented in Figure 4. Here temperature distribution is a decreasing function for higher ( $S_t = 0.3, 0.5, 0.7, 0.9$ ). In fact,  $(T_w - T_\infty)$  progressively decreases for increasing  $S_t$ , and hence the temperature profile  $\theta_1(\eta)$  decreases. In addition, an increase in parameter  $S_t$  causes the density of fluid layers to upsurge, resulting in dense ferrite particles to travel towards the surface, yielding increased magnetohydrodynamic interaction. This interaction causes the fluid viscosity to increase and the thermal conductivity to decrease, resulting in a reduction in heat transfer.

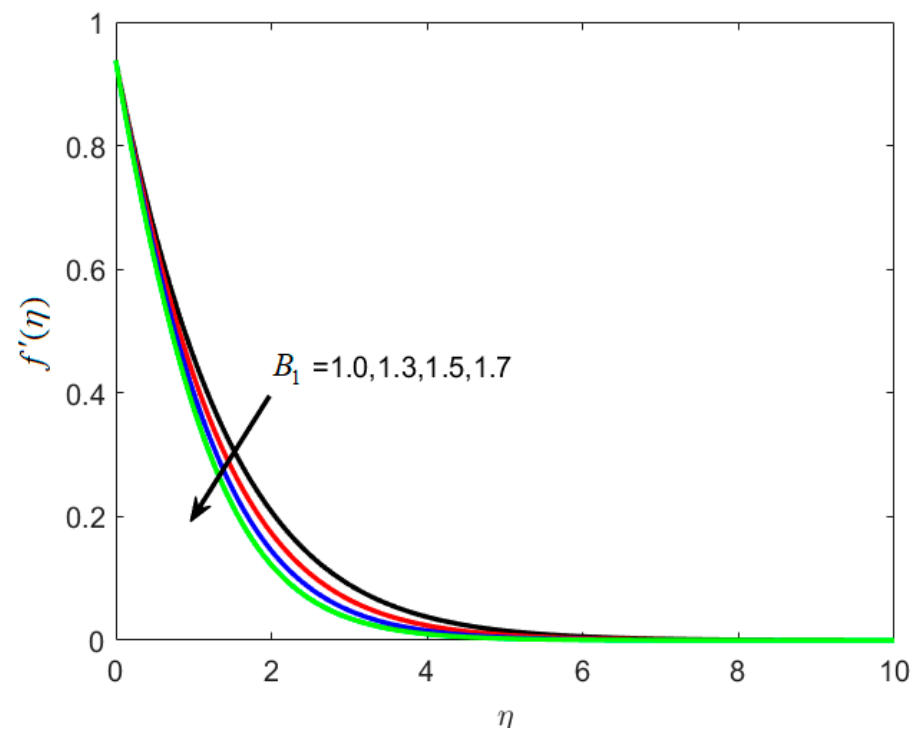


**Figure 2.** Various estimates of first material parameter  $B_1$  by taking  $B_2 = 1.2$ ,  $S_t = 0.3$ ,  $\lambda_h = 0.1$ ,  $N_c = 0.3$ ,  $N_t = 0.2$ ,  $\gamma = 0.2$ ,  $\kappa^* = 0.1$ ,  $Le = 0.2$ ,  $\delta = 0.3$ .

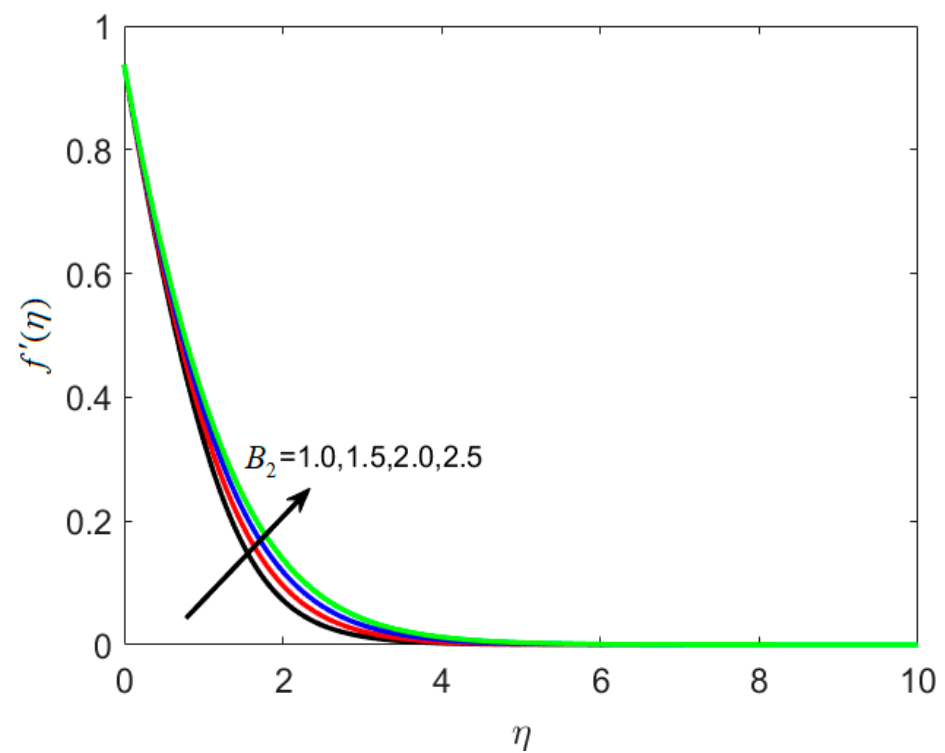


**Figure 3.** Various estimates of second material parameter  $B_2$  by taking  $B_1 = 1.2$ ,  $S_t = 0.3$ ,  $\lambda_h = 0.1$ ,  $N_c = 0.3$ ,  $N_t = 0.2$ ,  $\gamma = 0.2$ ,  $\kappa^* = 0.1$ ,  $Le = 0.2$ ,  $\delta = 0.3$ .

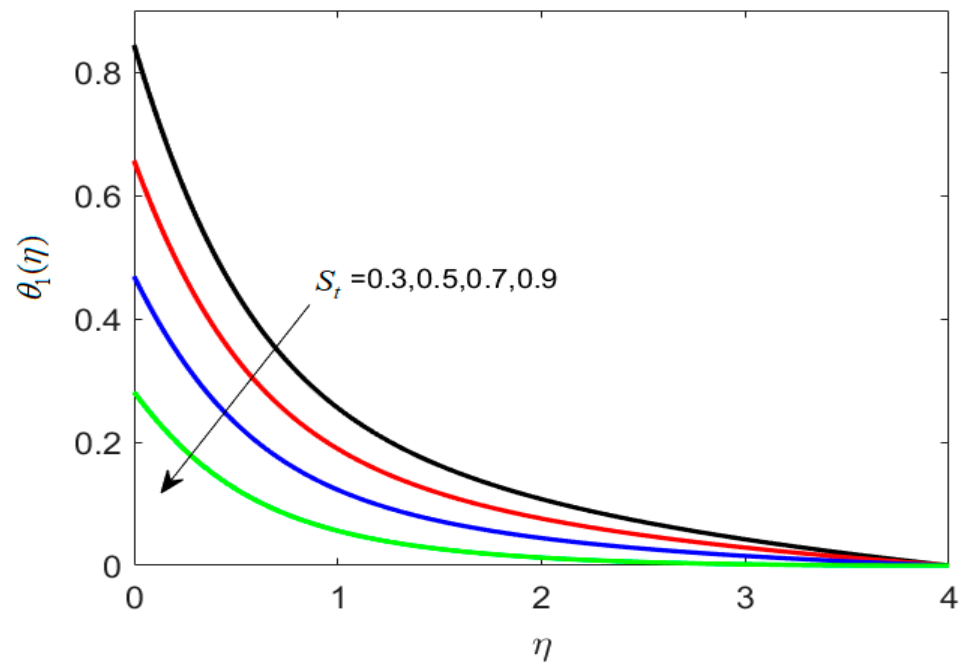


**Figure 4.** Different estimates of thermally stratified parameter  $S_t$  by taking  $B_1 = 1.2$ ,  $B_2 = 1.3$ ,  $\lambda_h = 0.1$ ,  $N_c = 0.3$ ,  $N_t = 0.2$ ,  $\gamma = 0.2$ ,  $\kappa^* = 0.1$ ,  $Le = 0.2$ ,  $\delta = 0.3$ .

Figure 5 illustrates the consequence of the thermal relaxation time parameter  $\lambda_h$  on  $\theta_1(\eta)$ . As seen in Figure 5, a decrease in temperature is noticed with increases in ( $\lambda_h = 0.3, 0.5, 0.9, 1.2$ ) (thermal relaxation time parameter). Because of the extended thermal relaxation period, the fluid temperature drops. This effect necessitates additional time for heat to be transported to nearby particles, which gives rise to magnetohydrodynamic interactions, and heat transfer reduces.

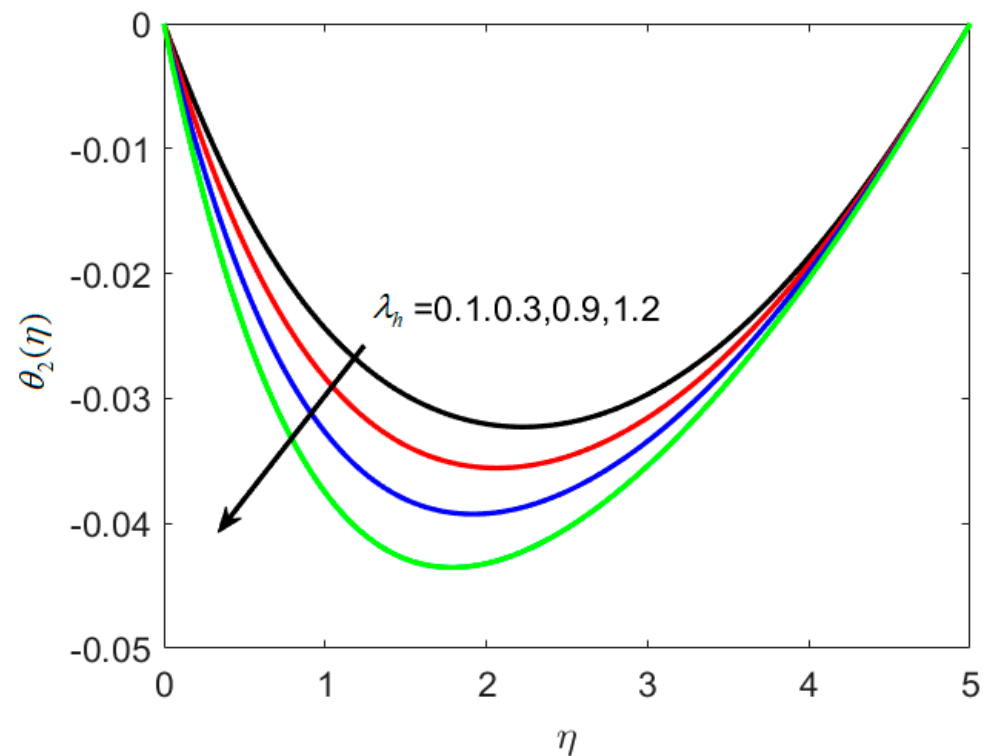


**Figure 5.** Various estimates of the thermal relaxation time parameter  $\lambda_h$  by taking  $B_1 = 1.2$ ,  $B_2 = 1.3$ ,  $S_t = 0.3$ ,  $N_c = 0.3$ ,  $N_t = 0.2$ ,  $\gamma = 0.2$ ,  $\kappa^* = 0.1$ ,  $Le = 0.2$ ,  $\delta = 0.3$ .

### 8.3. Concentration and Microorganism Profiles

On the concentration graph, Figure 6 depicts the fluctuation of thermophoretic parameter  $N_t$ . It is worth noting that as  $N_t$  increases, the concentration profile decreases, and the thickness of the layer decreases. In addition, when the engorged value of  $N_t$  is taken, more nanoparticles are pushed away from the heated surface. The reason is that when the fluid heats up it becomes thin on the increment of thermophoresis. The rise in the thermophoresis parameter has a direct influence on the flow of nanoparticles towards the cold section, resulting in a reduction in nanoparticle concentration in the fluid. Differing trends of dimensionless concentration ratio parameter  $N_c$  against  $\Omega_1(\eta)$  are seen in Figure 7. The concentration of the fluid is increased with amplified  $N_c$ . The reason is that particles are engaged in the opposite path of the concentration gradient by the concentration ratio parameters, which causes the nanofluid to become more homogenous. Figure 8 is used to show the effect of dimensionless reaction rate constant  $\gamma$  on  $\Omega_2(\eta)$ . For large rate constant values  $\gamma$ , it is understood that concentration deteriorates. Large estimations of  $\gamma$  give a decreased concentration profile, which strengthens the decreased chemical reaction in the end.

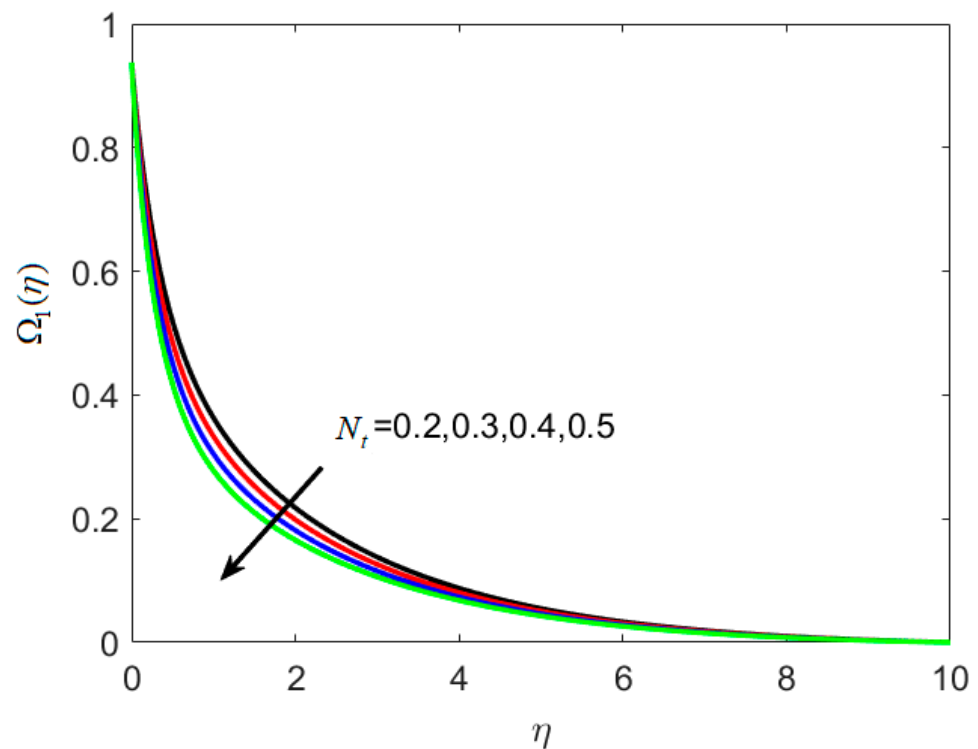


**Figure 6.** Various estimates of thermophoretic parameter  $N_t$  by taking  $B_1 = 1.3$ ,  $B_2 = 1.2$ ,  $S_t = 0.3$ ,  $\lambda_h = 0.1$ ,  $N_c = 0.3$ ,  $\gamma = 0.2$ ,  $\kappa^* = 0.1$ ,  $Le = 0.2$ ,  $\delta = 0.3$ .

The concentration profile is affected by the thermophoretic coefficient,  $\Omega_2(\eta)$ , as seen in Figure 9, which is a rising function of  $\kappa^*$  in this case. When microscopic particles are exposed to a cold surface, thermophoresis produces a suction-like effect on them. This research helps to regulate the heat gradient of a microfluidic size, which is extensively used in microdevices. Decreasing the temperature of the densest ferrite particles results in an increasing concentration boundary layer. Figure 10 shows the impact of  $Le$  on  $\chi_1(\eta)$ . For higher values of  $Le$ , the microorganisms' diffusivity drops, and this results in the reduction of the density of liquid particles. It is illustrated in Figure 11 that boosting  $\delta$  decreases  $\chi_2(\eta)$  because the density of motile microorganisms reduces in the nanofluid flow with increasing  $\delta$ . Therefore, higher  $\delta$  produces a rapid reduction in the  $\chi_2(\eta)$ , because  $\delta$  opposes the fluid motion.

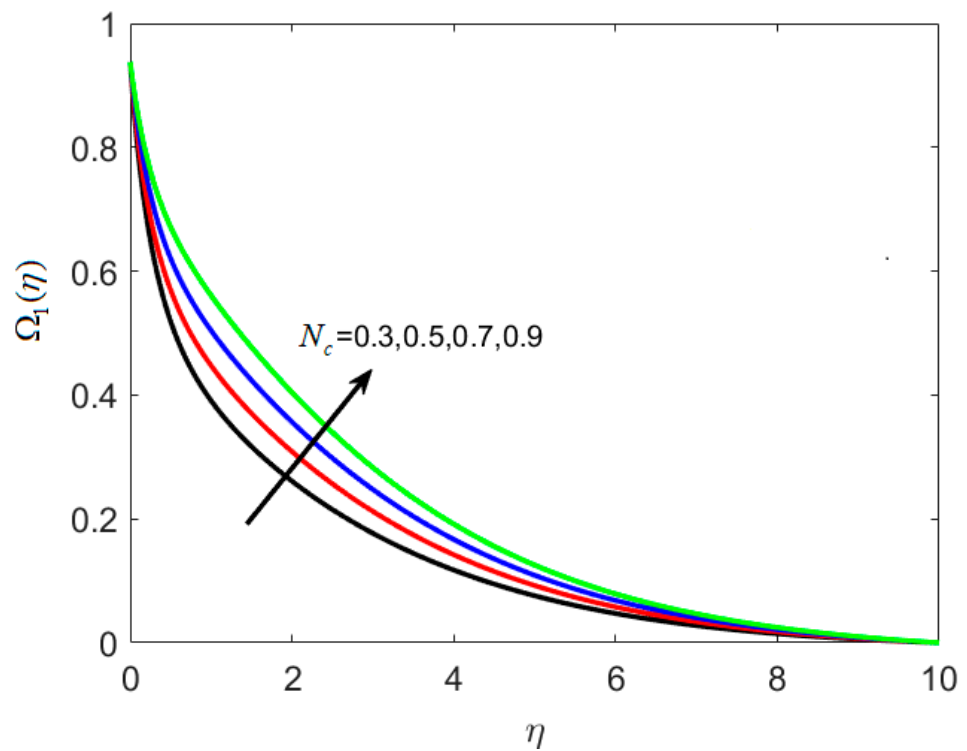


**Figure 7.** Various estimates of dimensionless concentration ratio parameter  $N_c$  by taking  $B_1 = 1.3$ ,  $B_2 = 1.2$ ,  $S_t = 0.3$ ,  $\lambda_h = 0.1$ ,  $N_t = 0.3$ ,  $\gamma = 0.2$ ,  $\kappa^* = 0.1$ ,  $Le = 0.2$ ,  $\delta = 0.3$ .

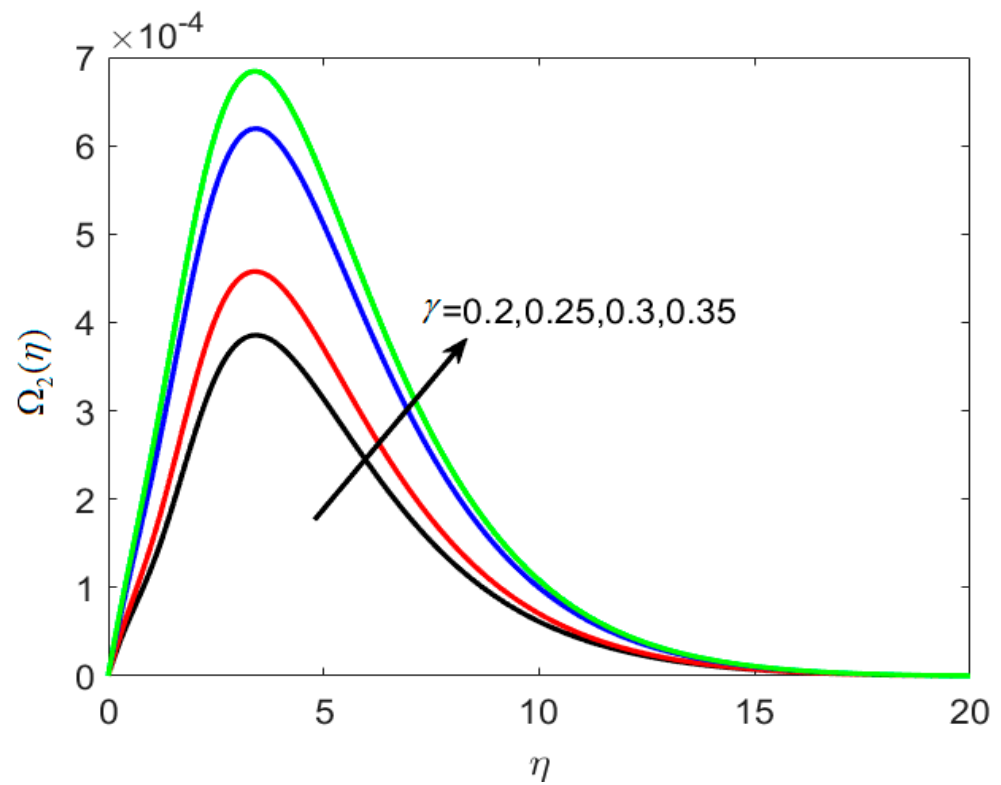


**Figure 8.** Various estimates of dimensionless reaction rate constant  $\gamma$  by taking  $B_1 = 1.3$ ,  $B_2 = 1.2$ ,  $S_t = 0.3$ ,  $\lambda_h = 0.1$ ,  $N_t = 0.3$ ,  $N_c = 0.3$ ,  $\kappa^* = 0.1$ ,  $Le = 0.2$ ,  $\delta = 0.3$ .

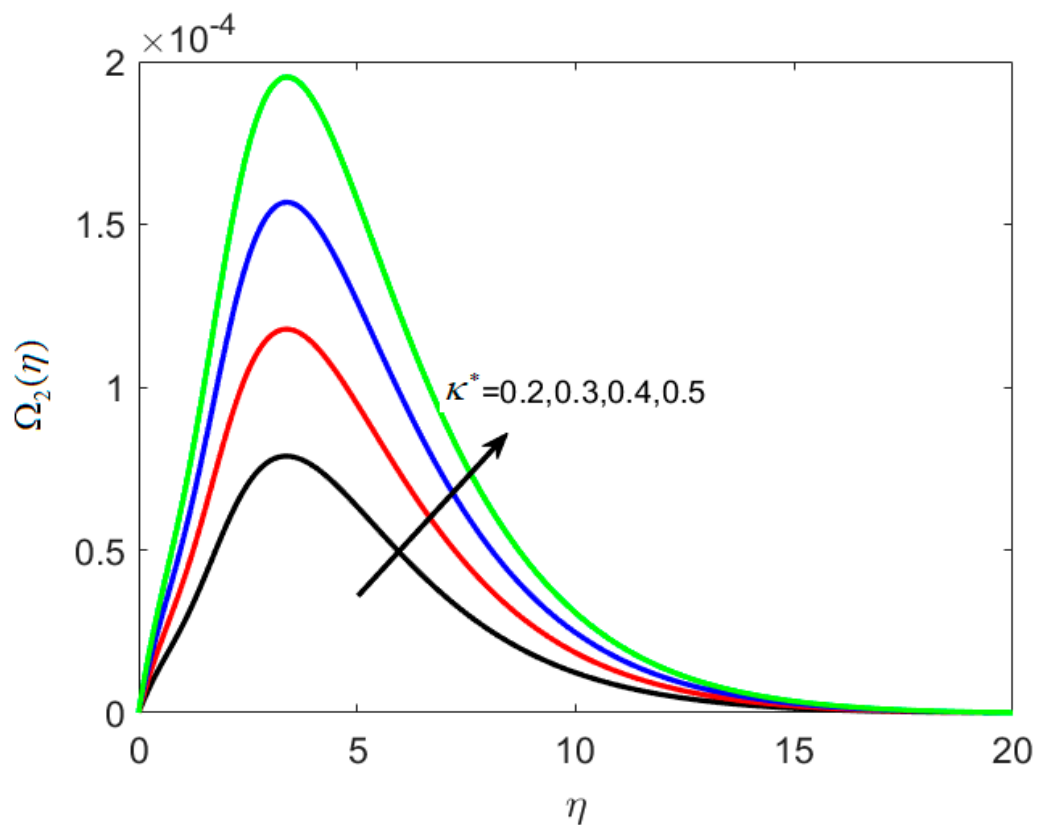


**Figure 9.** Various estimates of thermophoretic coefficient  $\kappa^*$  by taking  $B_1 = 1.3, B_2 = 1.2, S_t = 0.3, \lambda_h = 0.1, N_t = 0.3, N_c = 0.3, \gamma = 0.2, Le = 0.2, \delta = 0.3$ .

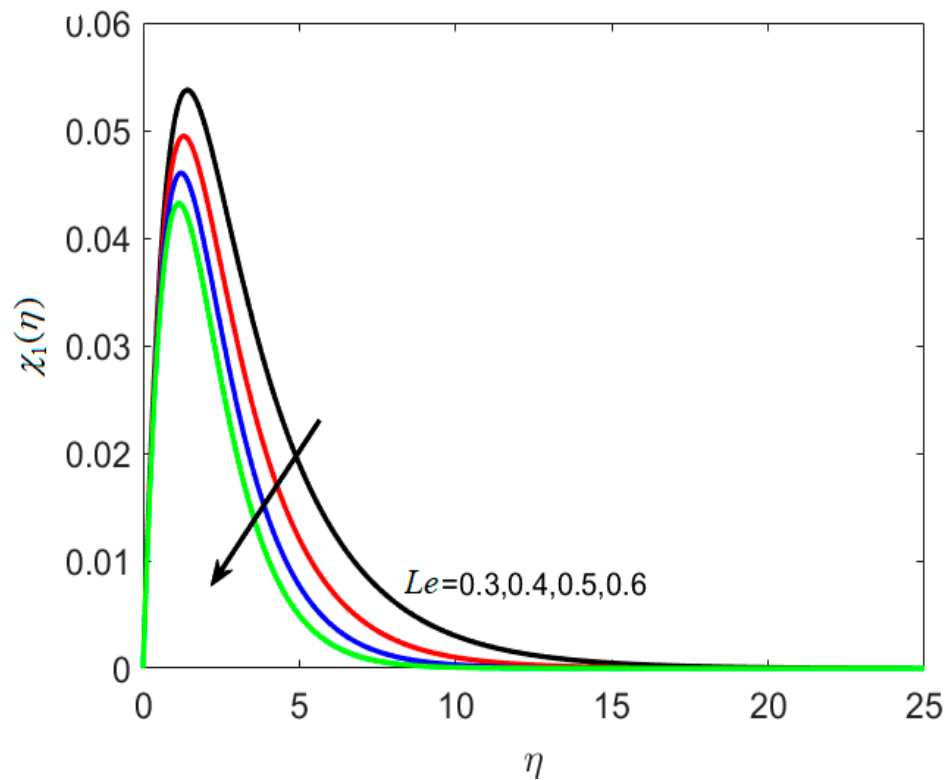


**Figure 10.** Various estimates of Lewis number  $Le$  by taking  $B_1 = 1.3, B_2 = 1.2, S_t = 0.3, \lambda_h = 0.1, N_t = 0.3, N_c = 0.3, \kappa^* = 0.1, \gamma = 0.2, \delta = 0.3$ .

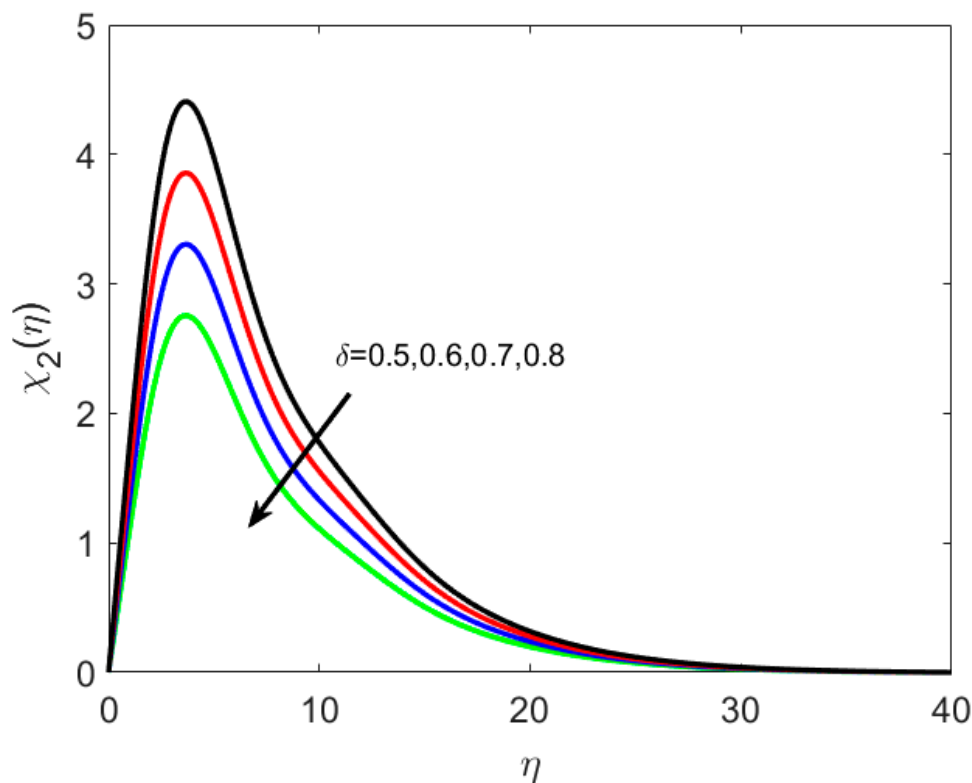


**Figure 11.** Various estimates of solutal relaxation parameter  $\delta$  by taking  $B_1 = 1.3, B_2 = 1.2, S_t = 0.3, \lambda_h = 0.1, N_t = 0.3, N_c = 0.3, \kappa^* = 0.1, Le = 0.2, \gamma = 0.2$ .

Numerical values of  $N_u, St_r,$  and  $N_n$  are displayed in Tables 2–4, respectively. It is evident from Table 2 that the transfer of heat rate coefficient  $N_u$  decreases with increasing  $\lambda_h, \alpha,$  and  $\eta,$  while its value surges with increasing  $\beta, \varepsilon,$  and  $\lambda.$  In addition, Table 3 indicates thermophoretic deposition velocity decreases with increasing  $Sc$  and  $\kappa^*.$  Table 4 shows that the density number of motile microorganisms decreases with increasing Peclet number  $Pe.$

**Table 2.** Estimation of Nusselt number ( $Nu_x Re_x^{\frac{1}{2}}$ ) for varying parameters  $\lambda_h, \beta, \varepsilon, Pr, \lambda, S_t, \alpha, \eta.$

$\lambda_h$	$\beta$	$\varepsilon$	$Pr$	$\lambda$	$S_t$	$\alpha$	$\eta$	$-(\theta'_1(0)+\zeta^2\theta'_2(0))$
0.5	1.1	0.1	1.2	0.1	0.1	0.3	1.1	1.1007748
0.6								1.0969643
0.7								1.0838647
	1.2							1.1008176
	1.3							1.1008605
		0.2						1.1016806
		0.3						1.1025864
			1.3					1.1460540
			1.4					1.1885233
				0.2				1.1021934
				0.3				1.1036116
					0.2			1.1906204
					0.3			1.2804782
						0.4		1.1006387
						0.5		1.1005585
							1.2	1.1006819
							1.3	1.1006387
					1.1			0.20969592
					1.2			0.2145712

**Table 3.** Numerical estimation of local Stanton number ( $St_f R_{ex}^{\frac{1}{2}}$ ) for different parameters  $\gamma, N_c, N_t, Sc, k^*$ .

$\gamma$	$N_c$	$N_t$	$Sc$	$k^*$	$-\frac{(\Omega'_1(0)+\xi^2\Omega'_2(0))}{Sc}$
0.7	1.3	0.1	0.4	1.5	1.4893254
0.8					1.5668322
0.9					1.6394216
	1.4				1.4763646
	1.5				1.4634038
		0.2			1.4392334
		0.3			1.3787588
			0.5		1.3458035
			0.6		1.245990
				1.6	1.4864837
				1.7	1.4836393

**Table 4.** Numerical estimation of the number density of microorganisms ( $N_n R_{ex}^{-\frac{1}{2}}$ ) for different parameters  $Le, \delta, Pe$ .

$Le$	$\delta$	$Pe$	$-(\chi'_1(0)+\xi^2\chi'_2(0))$
0.2	0.5	1.1	-0.28919802
0.3			-0.28562933
0.4			-0.2809328
	0.6		-0.34703762
	0.7		-0.40487721
		1.2	-0.31631026
		1.3	-0.3435266

Table 5 shows the comparison of  $-f''(0)$  with available published work by setting  $Pr = 1, \frac{1}{\beta^*} \rightarrow 0$ , and ignoring  $B_1, B_2, \lambda, \beta, \lambda_h$ . Good agreement is observed with already published work, which increases the validity, credibility, and the accuracy of the present work.

**Table 5.** Comparison of  $-f''(0)$  with available published work by suppressing the additional parameters. Selecting  $Pr = 1, \frac{1}{\beta^*} \rightarrow 0$ , and considering  $B_1 = B_2 = \lambda, = \beta, = \lambda_h = 0$ .

Published Articles	$-f''(0)$
Chen et al. [29]	0.6012011
Kumar et al. [17]	0.6069352
Pal et al. [46]	0.615066
Zeeshan et al. [48]	0.6058427
Present	0.6012541

### 9. Concluding Remarks

In this investigation, we explored the impact of magnetic dipole and thermophoretic particle deposition on Oldroyd-B fluid flow over a stretching sheet. In the proposed model, to analyze the heating mechanism, the Cattaneo–Christov heat flux model is added to an electrically non-conducting, thermally stratified ferromagnetic nanofluid. Magnetic dipole effects are also taken into account. Additionally, the concentration field is inspected under consideration of thermophoretic particle deposition and chemical reaction. Gyrotactic microorganisms of Oldroyd-B nanofluid are employed in order to stabilize the suspended ferromagnetic particles. The following are the problem’s most notable outcomes:

- The opposite behavior of velocity function  $f'(\eta)$  is observed with increasing relaxation retardation time constants  $B_1$  and  $B_2$ .
- Thermal stratification parameter  $S_t$  minimizes temperature profiles.
- $\Omega_1$  and  $\Omega_2$  decrease with increasing  $N_t$ .

- Thermal relaxation parameter  $\lambda_h$  decreases the temperature profiles.
- $N_u$  increases with increasing  $\beta$ .
- Large estimations of  $\gamma$  decrease the concentration profile.
- Thermophoretic deposition velocity decreases with increasing  $Sc$  and  $\kappa^*$ .
- The density number of motile microorganisms decreases with increasing  $Pe$  and  $Le$ .

**Author Contributions:** M.R. supervised and considered the idea; S.B. wrote the manuscript; H.A.S.G. worked on the software; K.S.N., C.A.S. and A.A. helped in editing and validation. All authors have read and agreed to the published version of the manuscript.

**Funding:** The authors extend their appreciation to the Deanship of Scientific Research at King Khalid University, Saudi Arabia, for funding this work through the Research Group Program under Grant No: RGP 2/26/43.

**Data Availability Statement:** The datasets used and/or analyzed during the current study are available from the corresponding author on reasonable request.

**Conflicts of Interest:** The authors declare that they have no known competing financial interests or personal relationships that could have appeared to influence the work reported in this paper.

## Nomenclature

$c$	Constant	$\tilde{u}, \tilde{v}$	Velocity components $m/s$
$V_T$	Thermophoretic velocity	$V_d$	Thermophoretic deposition velocity $m/s$
$x, y$	Coordinates axis $m$	$C$	Concentration $m^{-3}mol$
$N_t$	Thermophoretic parameter	$V_d^*$	Non-dimensional thermophoretic deposition velocity
$N_c$	Dimensionless concentration ratio	$T$	Temperature $K$
$b$	Chemotaxis constant	<b>Greek symbols</b>	
$T_c$	Curie temperature $K$	$\lambda$	Viscous dissipation parameter
$W_e$	Highest swimming speed of microorganisms	$\tau_w, q_h, q_m$	Shear stress, surface heat flux, surface mass flux
$k$	Thermal conductivity $W m^{-1}K^{-1}$	$\lambda_H$	Thermal relaxation time coefficient
$M$	Magnetization $m^{-2}Wb$	$\mu_0$	Free space permeability $A^{-2}N$
$Sc$	Schmidt number	$\tilde{\Lambda}_1, \tilde{\Lambda}_2$	Relaxation, retardation times of material parameters
$f(\eta)$	Dimensionless velocity	$K$	Gyromagnetic coefficient
$S_t$	Thermal stratification parameter	$\gamma_0$	Strength of magnetic field $cm$
$L_e$	Traditional Lewis number	$\gamma$	Dimensionless reaction rate constant
$e$	Distance $cm$	$\delta$	Solutal relaxation parameter
$\tilde{H}$	Magnetic field	$\mu$	Dynamic viscosity $m^2s^{-1}$
$T_w$	Wall temperature $K$	$\theta_1(\eta), \theta_2(\eta)$	Dimensionless temperature
$B_1, B_2$	Deborah numbers or dimensionless material parameters	$\beta$	Ferromagnetic interaction parameter
$Pe$	Bioconvection Peclet number	$n_w$	Diffusive concentration of microorganisms at the wall
$k_1^*$	Chemical reaction rate	$\eta, \zeta$	Similarity variables
$Pr$	Prandtl number	$v$	Kinematic viscosity $m^2s^{-1}$
$Re_x$	Local Reynolds number	$\alpha$	Dimensionless distance
$\kappa^*$	Thermophoretic coefficient	$\Omega_1(\eta), \Omega_2(\eta)$	Dimensionless concentration
$St_r$	Local Stranton number	$\varphi$	Scalar potential
$D$	Diffusion coefficient $m^2s^{-1}$	$\varepsilon$	Dimensionless curie temperature
$N_u$	Local Nusselt number	$\rho$	Density $kgm^{-3}$
$N_n$	Density of motile microorganisms	$\beta^*$	Fluid parameter
$K_n$	Knudsen number	$\varphi$	Scalar potential
$n_1, n_2$	Constants	$\lambda_h$	Thermal relaxation parameter
$T_0$	Reference temperature $K$	$\chi_1(\eta), \chi_2(\eta)$	Dimensionless diffusive concentration of microorganisms
$C_p$	Specific heat capacity $J/(K kg)$	$\chi_1(\eta), \chi_2(\eta)$	Dimensionless diffusive concentration of microorganisms
$C_f$	Skin friction coefficient	$\alpha^*$	Thermal diffusivity $m^2s^{-1}$
$C_0$	Reference concentration $m^{-3}mol$		

## References

1. Oldroyd, J.G. On the formulation of rheological equations of state. *Proc. R. Soc. Lond. Ser. A Math. Phys. Sci.* **1950**, *200*, 523–541. [[CrossRef](#)]
2. Ibrahim, W.; Sisay, G.; Gamachu, D. Mixed convection flow of Oldroyd-B nano fluid with Cattaneo–Christov heat and mass flux model with third order slip. *AIP Adv.* **2019**, *9*, 125023. [[CrossRef](#)]
3. Hayat, T.; Imtiaz, M.; Alsaedi, A. Boundary layer flow of Oldroyd-B fluid by exponentially stretching sheet. *Appl. Math. Mech.* **2016**, *37*, 573–582. [[CrossRef](#)]
4. Ramzan, M.; Howari, F.; Chung, J.D.; Kadry, S.; Chu, Y.-M. Irreversibility minimization analysis of ferromagnetic Oldroyd-B nanofluid flow under the influence of a magnetic dipole. *Sci. Rep.* **2021**, *11*, 4810. [[CrossRef](#)]
5. Waqas, M.; Khan, M.I.; Hayat, T.; Alsaedi, A. Stratified flow of an Oldroyd-B nanoliquid with heat generation. *Results Phys.* **2017**, *7*, 2489–2496. [[CrossRef](#)]
6. Shehzad, S.; Abbasi, F.; Hayat, T.; Alsaedi, A. Cattaneo–Christov heat flux model for Darcy–Forchheimer flow of an Oldroyd-B fluid with variable conductivity and non-linear convection. *J. Mol. Liq.* **2016**, *224*, 274–278. [[CrossRef](#)]
7. Riaz, M.B.; Siddique, I.; Saeed, S.T.; Atangana, A. MHD Oldroyd-B Fluid with Slip Condition in view of Local and Nonlocal Kernels. *J. Appl. Comput. Mech.* **2020**, *7*, 116–127. [[CrossRef](#)]
8. Hafeez, A.; Khan, M.; Ahmed, J. Stagnation point flow of radiative Oldroyd-B nanofluid over a rotating disk. *Comput. Methods Programs Biomed.* **2020**, *191*, 105342. [[CrossRef](#)]
9. Ramzan, M.; Bilal, M.; Chung, J.D. Radiative Williamson nanofluid flow over a convectively heated Riga plate with chemical reaction—A numerical approach. *Chin. J. Phys.* **2017**, *55*, 1663–1673. [[CrossRef](#)]
10. Lu, D.; Ramzan, M.; Bilal, M.; Chung, J.D.; Farooq, U.; Tahir, S. On three-dimensional MHD Oldroyd-B fluid flow with nonlinear thermal radiation and homogeneous–heterogeneous reaction. *J. Braz. Soc. Mech. Sci. Eng.* **2018**, *40*, 387. [[CrossRef](#)]
11. Saqib, M.; Khan, I.; Chu, Y.-M.; Qushairi, A.; Shafie, S.; Nisar, K.S. Multiple Fractional Solutions for Magnetic Bio-Nanofluid Using Oldroyd-B Model in a Porous Medium with Ramped Wall Heating and Variable Velocity. *Appl. Sci.* **2020**, *10*, 3886. [[CrossRef](#)]
12. Khan, M.N.; Nadeem, S.; Ullah, N.; Saleem, A. Theoretical treatment of radiative Oldroyd-B nanofluid with microorganism pass an exponentially stretching sheet. *Surf. Interf.* **2020**, *21*, 100686. [[CrossRef](#)]
13. Waqas, H.; Imran, M.; Muhammad, T.; Sait, S.M.; Ellahi, R. Numerical investigation on bioconvection flow of Oldroyd-B nanofluid with nonlinear thermal radiation and motile microorganisms over rotating disk. *J. Therm. Anal. Calorim.* **2021**, *145*, 523–539. [[CrossRef](#)]
14. Alam, M.; Rahman, M.; Sattar, M. Effects of variable suction and thermophoresis on steady MHD combined free-forced convective heat and mass transfer flow over a semi-infinite permeable inclined plate in the presence of thermal radiation. *Int. J. Therm. Sci.* **2008**, *47*, 758–765. [[CrossRef](#)]
15. Damseh, R.A.; Tahat, M.S.; Benim, D.-I.H.A.C. Nonsimilar solutions of magnetohydrodynamic and thermophoresis particle deposition on mixed convection problem in porous media along a vertical surface with variable wall temperature. *Prog. Comput. Fluid Dyn. Int. J.* **2009**, *9*, 58. [[CrossRef](#)]
16. Gowda, R.P.; Kumar, R.N.; Aldalbahi, A.; Issakhov, A.; Prasannakumara, B.; Rahimi-Gorji, M.; Rahaman, M. Thermophoretic particle deposition in time-dependent flow of hybrid nanofluid over rotating and vertically upward/ downward moving disk. *Surf. Interf.* **2021**, *22*, 100864. [[CrossRef](#)]
17. Kumar, R.N.; Jyothi, A.; Alhumade, H.; Gowda, R.P.; Alam, M.M.; Ahmad, I.; Gorji, M.; Prasannakumara, B. Impact of magnetic dipole on thermophoretic particle deposition in the flow of Maxwell fluid over a stretching sheet. *J. Mol. Liq.* **2021**, *334*, 116494. [[CrossRef](#)]
18. Kumar, R.N.; Gowda, R.J.P.; Madhukesh, J.K.; Prasannakumara, B.C.; Ramesh, G.K. Impact of thermophoretic particle deposition on heat and mass transfer across the dynamics of Casson fluid flow over a moving thin needle. *Phys. Scr.* **2021**, *96*, 075210. [[CrossRef](#)]
19. Khan, N.A.; Sultan, F.; Khan, N.A. Heat and mass transfer of thermophoretic MHD flow of Powell–Eyring fluid over a vertical stretching sheet in the presence of chemical reaction and Joule heating. *Int. J. Chem. React. Eng.* **2015**, *13*, 37–49. [[CrossRef](#)]
20. Alam, M.S.; Rahman, M.M.; Uddin, M.J.; Vajravelu, K. Numerical study of transient hydromagnetic forced convective slip flow over a porous rotating disk with thermophoresis. *J. Nonlinear Evol. Equ. Appl.* **2016**, *2016*, 1–23.
21. Shehzad, S.; Alsaedi, A.; Hayat, T.; Alhuthali, M. Thermophoresis particle deposition in mixed convection three-dimensional radiative flow of an Oldroyd-B fluid. *J. Taiwan Inst. Chem. Eng.* **2014**, *45*, 787–794. [[CrossRef](#)]
22. Doh, D.; Muthamilselvan, M. Thermophoretic particle deposition on magnetohydrodynamic flow of micropolar fluid due to a rotating disk. *Int. J. Mech. Sci.* **2017**, *130*, 350–359. [[CrossRef](#)]
23. Postelnicu, A. Thermophoresis particle deposition in natural convection over inclined surfaces in porous media. *Int. J. Heat Mass Transf.* **2012**, *55*, 2087–2094. [[CrossRef](#)]
24. Neuringer, J.L. Some viscous flows of a saturated ferro-fluid under the combined influence of thermal and magnetic field gradients. *Int. J. Non-Linear Mech.* **1966**, *1*, 123–137. [[CrossRef](#)]
25. Andersson, H.I.; Valnes, O.A. Flow of a heated ferrofluid over a stretching sheet in the presence of a magnetic dipole. *Acta Mech.* **1998**, *128*, 39–47. [[CrossRef](#)]
26. Waqas, M.; Jabeen, S.; Hayat, T.; Khan, M.I.; Alsaedi, A. Modeling and analysis for magnetic dipole impact in nonlinear thermally radiating Carreau nanofluid flow subject to heat generation. *J. Magn. Magn. Mater.* **2019**, *485*, 197–204. [[CrossRef](#)]

27. Gul, H.; Ramzan, M.; Nisar, K.S.; Mohamed, R.N.; Ghazwani, H.A.S. Performance-based comparison of Yamada–Ota and Hamilton–Crosser hybrid nanofluid flow models with magnetic dipole impact past a stretched surface. *Sci. Rep.* **2022**, *12*, 29. [[CrossRef](#)]
28. Bognár, G.; Hriczó, K. Ferrofluid flow in magnetic field above stretching sheet with suction and injection. *Math. Model. Anal.* **2020**, *25*, 461–472. [[CrossRef](#)]
29. Chen, S.B.; Shahmir, N.; Ramzan, M.; Sun, Y.L.; Aly, A.A.; Malik, M.Y. Thermophoretic particle deposition in the flow of dual stratified Casson fluid with magnetic dipole and generalized Fourier's and Fick's laws. *Case Stud. Therm. Eng.* **2021**, *26*, 101186. [[CrossRef](#)]
30. Kefayati, G. Natural convection of ferrofluid in a linearly heated cavity utilizing LBM. *J. Mol. Liq.* **2014**, *191*, 1–9. [[CrossRef](#)]
31. Ijaz, M.; Ayub, M. Simulation of magnetic dipole and dual stratification in radiative flow of ferromagnetic Maxwell fluid. *Heliyon* **2019**, *5*, e01465. [[CrossRef](#)] [[PubMed](#)]
32. Alshomrani, A.S.; Ramzan, M. Upshot of magnetic dipole on the flow of nanofluid along a stretched cylinder with gyrotactic microorganism in a stratified medium. *Phys. Scr.* **2019**, *95*, 025702. [[CrossRef](#)]
33. Ahmad, S.; Khan, M.N.; Rehman, A.; Felemban, B.F.; Alqurashi, M.S.; Alharbi, F.M.; Alotaibi, F.; Galal, A.M. Analysis of Heat and Mass Transfer Features of Hybrid Casson Nanofluid Flow with the Magnetic Dipole Past a Stretched Cylinder. *Appl. Sci.* **2021**, *11*, 11203. [[CrossRef](#)]
34. Shah, Z.; Vrinceanu, N.; Rooman, M.; Deebani, W.; Shutaywi, M. Mathematical Modelling of Ree-Eyring Nanofluid Using Koo-Kleinstreuer and Cattaneo–Christov Models on Chemically Reactive AA7072-AA7075 Alloys over a Magnetic Dipole Stretching Surface. *Coatings* **2022**, *12*, 391. [[CrossRef](#)]
35. Nisar, K.S.; Khan, U.; Zaib, A.; Khan, I.; Baleanu, D. Exploration of aluminum and titanium alloys in the stream-wise and secondary flow directions comprising the significant impacts of magnetohydrodynamic and hybrid nanofluid. *Crystals* **2020**, *10*, 679. [[CrossRef](#)]
36. Abbasi, F.M.; Shehzad, S.A.; Hayat, T.; Alhuthali, M.S. Mixed convection flow of jeffrey nanofluid with thermal radiation and double stratification. *J. Hydrodyn. Ser. B* **2016**, *28*, 840–849. [[CrossRef](#)]
37. Sandeep, N.; Sulochana, C. Dual solutions for unsteady mixed convection flow of MHD micropolar fluid over a stretching/shrinking sheet with non-uniform heat source/sink. *Eng. Sci. Technol. Int. J.* **2015**, *18*, 738–745. [[CrossRef](#)]
38. Ramzan, M.; Liaquet, A.; Kadry, S.; Yu, S.; Nam, Y.; Lu, D. Impact of Second-Order Slip and Double Stratification Coatings on 3D MHD Williamson Nanofluid Flow with Cattaneo–Christov Heat Flux. *Coatings* **2019**, *9*, 849. [[CrossRef](#)]
39. Rehman, K.U.; Malik, M.; Salahuddin, T.; Naseer, M. Dual stratified mixed convection flow of Eyring–Powell fluid over an inclined stretching cylinder with heat generation/absorption effect. *AIP Adv.* **2016**, *6*, 075112. [[CrossRef](#)]
40. Kandasamy, R.; Dharmalingam, R.; Prabhu, K.S. Thermal and solutal stratification on MHD nanofluid flow over a porous vertical plate. *Alex. Eng. J.* **2018**, *57*, 121–130. [[CrossRef](#)]
41. Khan, M.; Rasheed, A.; Salahuddin, T.; Ali, S. Chemically reactive flow of hyperbolic tangent fluid flow having thermal radiation and double stratification embedded in porous medium. *Ain Shams Eng. J.* **2021**, *12*, 3209–3216. [[CrossRef](#)]
42. Mallawi, F.; Bhuvaneswari, M.; Sivasankaran, S.; Eswaramoorthi, S. Impact of double-stratification on convective flow of a non-Newtonian liquid in a Riga plate with Cattaneo–Christov double-flux and thermal radiation. *Ain Shams Eng. J.* **2021**, *12*, 969–981. [[CrossRef](#)]
43. Bilal, M.; Ramzan, M.; Mehmood, Y.; Alaoui, M.K.; Chinram, R. An entropy optimization study of non-Darcian magnetohydrodynamic Williamson nanofluid with nonlinear thermal radiation over a stratified sheet. *Proc. Inst. Mech. Eng. Part E J. Process. Mech. Eng.* **2021**, *235*, 1883–1894. [[CrossRef](#)]
44. Ramzan, M.; Ullah, N.; Chung, J.D.; Lu, D.; Farooq, U. Buoyancy effects on the radiative magneto Micropolar nanofluid flow with double stratification, activation energy and binary chemical reaction. *Sci. Rep.* **2017**, *7*, 12901. [[CrossRef](#)] [[PubMed](#)]
45. Bilal, M.; Ramzan, M.; Mehmood, Y.; Sajid, T.; Shah, S.; Malik, M.Y. A novel approach for EMHD Williamson nanofluid over nonlinear sheet with double stratification and Ohmic dissipation. *Proc. Inst. Mech. Eng. Part E J. Process Mech. Eng.* **2021**. [[CrossRef](#)]
46. Pal, D.; Mondal, H. Hydromagnetic non-Darcy flow and heat transfer over a stretching sheet in the presence of thermal radiation and Ohmic dissipation. *Commun. Nonlinear Sci. Numer. Simul.* **2010**, *15*, 1197–1209. [[CrossRef](#)]
47. Tlili, I.; Naseer, S.; Ramzan, M.; Kadry, S.; Nam, Y. Effects of chemical species and nonlinear thermal radiation with 3D Maxwell nanofluid flow with double stratification—An analytical solution. *Entropy* **2020**, *22*, 453. [[CrossRef](#)]
48. Zeeshan, A.; Majeed, A. Effect of magnetic dipole on radiative non-Darcian mixed convective flow over a stretching sheet in porous medium. *J. Nanofluids* **2016**, *5*, 617–626. [[CrossRef](#)]